International Journal of Natural and Engineering Sciences 8 (2): 30-34, 2014
ISSN: 1307-1149, E-ISSN: 2146-0086, www.nobel.gen.tr

Steady-State Analysis and Simulation of Raman Laser Based on HNL-PCF

Sarah BARZEGAR[1*] Ghafar DARVISH[1]

[1]Department of Electrical Engineering, Science and Research Branch, Islamic Azad University, Tehran, IRAN

*Corresponding author:
E-mail: s.barzegar@srbiau.ac.ir

Received: June 15, 2014
Accepted: August 07, 2014

Abstract

In this paper, we investigate numerically steady-state behavior of a highly nonlinear photonic crystal fiber (PCF) Raman laser. The threshold power proportional photonic crystal fiber length has been studied. As well as, two types of Raman fiber lasers (RFLs), with- and without Bragg gratings have been compared. Calculations are performed using Runge-Kutta method. Transmission power and output power of the 2nd-order Stokes radiation toward input pump power for low-reflectivity mirrors cascade Raman resonator have been presented. Moreover, forward propagation of the 1st-order Stokes wave changes have been shown as indicator for satisfactory output power in the acceptable rang of the PCF length. We explain trade-off between attenuation dependence of effective length and output power. Finally, output power versus reflection- and transmission coefficients before fiber-end facet has been described.

Keywords: Raman Fiber Laser, Photonic Crystal Fiber, Stokes Waves, Bragg Grating

INTRODUCTION

Nowadays, photonic crystal fibers (PCFs) are used in constructing different optical sources such as Raman fiber lasers (RFLs) based on Raman Effect [1]. Already, reports obtained were found optimal output power for several-stop cascade in the nested fiber Raman cavity using Bragg reflectors all interactions between forward and backward travelling waves [2]. As well as, output power was adjusted by the reflectivity of the fiber grating output couplers [3] and some FBG characteristics, such as insertion losses [4].

Progresses of technology in create photonic crystal fibers were optimized whit variety of material doped, improvement fabrication, fundamental Rayleigh scattering characteristics and geometric parameters in structure of PCF [5,6]. RFLs with multi- wavelength output are important to the gain flattening and used as pumps for Raman amplifiers, are discussed [7-9]. Meanwhile, Raman fiber laser (RFL) is an attractive photon source in the fields of optical communication and optical sensors because of its flexibility to design all-fiber configuration [9].

On the other hand, a Raman linear cavity for multiwavelength generation [10] formed by an optical fiber of length L and two fiber Bragg gratings reflecting at the Stokes wavelength λ_p [11] with Reflectivity in two hand fiber ends.

Highly nonlinear photonic crystal fibers (HNL-PCFs) have recently emerged as promising gain media providing a strong confinement of light within a core which can be heavily GeO_2-doped to enhance the Raman gain. Also Bragg grating formed inside the core of the PCF [1]. RFL based on HNL-PCF considered as an appropriate power source with narrow spectrum in extensive range of wavelength. Stimulated Raman scattering (SRS) effect explained improvement behavior of high nonlinear-PCF Raman laser.

We investigate the first-order and the second-order Stokes waves threshold pump power variations as length of PCF for a novel structure RFL. Also, numerical analysis has been applied to calculated fundamental parameters of PCF Raman laser. In this work, nonlinear differential equations are solved by RK4. In addition, output power of the Raman fiber laser has been obtained for the grating-free and the Bragg grating mirrors. In this model, continues wave has been assumed at the first part of cavity.

The rest of this paper is organized as follows: in section 2, we present the theoretical background for a photonic crystal fiber Raman laser structure. In section 3, simulation of the steady state behaviors are accomplished by using RK method. Also, parameters of HNL-photonic crystal fiber laser have been calculated. Finally, we conclude this paper in section 4.

THEORETICAL BACKGROUND

The Raman fiber laser consists of three sections. The first portion is a set of multimode diodes that used as optical pumps. The next section is composed of rare-earth-doped cladding-pump fiber laser, which converts the multimode diode light into single mode light at another wavelength. Finally, this single mode light is converted to a desired wavelength by a cascaded Raman resonator [7]. In other word, the cascade Raman resonator is an important part of the complete RFL, which is used as cavity for lunched converted single mode continues light wave to the specific wavelength. Figure 1 illustrates a simple schematic of a linear cascaded cavity Raman fiber laser using FBGs as feedback elements made by a HNL-PCF. Two pairs of FBGs form the resonant cavities for the first and the second Stokes waves [12].

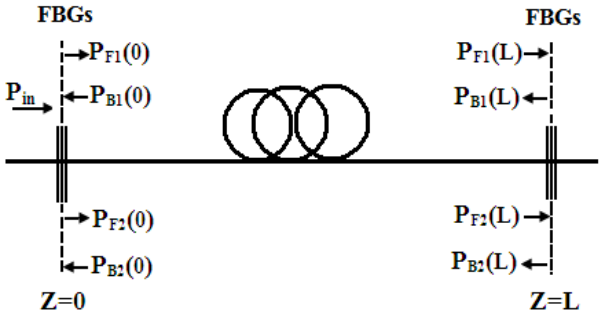

Figure 1. Configuration of Raman fiber laser fabricated with a HNL-PCF as cavity

The fiber laser converts pump wave to Stokes waves, gradually. The pump power injected at the left-hand side (at z=0) decreases toward larger z because it loses power to the forward- and backward propagating Stokes waves due to stimulated Raman scattering (SRS) [11]. It is described by the steady-state power distribution of each Raman order inside the RFL fiber cavity.

The coupled rate equations for forward- and backward propagating pump power and Stokes powers in Raman gain PCF are given by:

$$\frac{\partial P}{\partial z} = -\alpha_p P_p - g_{R1}\frac{\lambda_{s1}}{\lambda_p}(P_{F1} + P_{B1})Pp \quad (1)$$

$$\frac{\partial P_{F1}}{\partial z} = -\alpha_{s1}P_{F1} + g_{R1}P_pP_{F1} - g_{R2}\frac{\lambda_{s2}}{\lambda_{s1}}(P_{F2} + P_{B2})P_{F1} \quad (2)$$

$$-\frac{\partial P_{B1}}{\partial z} = -\alpha_{s1}P_{B1} + g_{R1}P_pP_{B1} - g_{R2}\frac{\lambda_{s2}}{\lambda_{s1}}(P_{F2} + P_{B2})P_{B1} \quad (3)$$

$$\frac{\partial P_{F2}}{\partial z} = -\alpha_{s2}P_{F2} + g_{R2}(P_{F1} + P_{B1})P_{F2} \quad (4)$$

$$-\frac{\partial P_{B2}}{\partial z} = -\alpha_{s2}P_{B2} + g_{R2}(P_{F1} + P_{B1})P_{B2} \quad (5)$$

In these equations P_{F1}, P_{B2}, P_{F2} and P_{B2} represent optical powers of the forward and backward propagating for the first- and second-order Stokes waves [1], respectively. α_p is related to amount of attenuation coefficient at the pump wavelength. Also, α_{s1} and α_{s2} show power attenuation coefficients at Stokes wavelength. λ_p, λ_{s1} and λ_{s2} illustrate the wavelength of pump power, for the 1st- and the 2nd-order Stokes waves, respectively. In these equations, g_{R1}, g_{R2} represent the Raman gain coefficients. These coefficients are increased linearly with the Germania concentration [5]. In fact, the Raman gain coefficients are independent of the geometrical parameters and just depend on the type and concentration of materials which form PCF.

The boundary conditions which describe the pump power that is injected into the PCF, forward and backward propagation powers at Stokes wavelengths in the z = 0 and z = L, can be written as:

$$P_p(0) = P_{inc} \quad (6)$$

$$P_{F1}(0) = R_{in1}F_{B1}(0) \quad (7)$$

$$P_{F2}(0) = R_{in2}P_{B2}(0) \quad (8)$$

$$P_{B1}(L) = R_{out1}P_{F1}(L) \quad (9)$$

$$P_{B2}(L) = R_{out2}P_{F2}(L) \quad (10)$$

Where P_{inc} shows the incident pump power, L represents the PCF length, distinctly. Bragg grating mirrors have been placed inside the core of the PCF [1]. Power radiations at the pump wavelength and Stokes wavelengths are formed and separated by FBG_0, FBG_1 and FBG_2. The Bragg gratings reflection coefficients are represented with R_{in1}, R_{in2} and the same kind, R_{out1}, R_{out2} for description of resonance in input and output mirrors, respectively.

SIMULATION RESULT

In this part the ability to obtain a combination of PCF-Raman fiber laser's parameters with- and without FBG for low threshold current and high output power by simulation is discussed. The germanium content in the doped section of the PCF core is about 25 Wt%. The core diameter of the PCF is about 2.5 μm. The power characteristics of this PCF such as optical losses are experimentally obtained [1]. Details of the parameters used in our numerical analysis have been summarized in Table 1.

Table 1.Highly Nonlinear-PCF Essential Parameters Used for Raman Laser [1]

Parameters		Values
Wavelength of Pump	λ_p(nm)	1064
Wavelength of 1st-order Stokes	λ_{s1}(nm)	1118
Wavelength of 2nd-order Stokes	λ_{s2}(nm)	1177
Attenuation Coefficient at λ_p	$\alpha p(km^{-1})$	2.21
Attenuation Coefficient at λ_{s1}	$\alpha s1(km^{-1})$	2.12
Attenuation Coefficient at λ_{s2}	$\alpha s2(km^{-1})$	2.03
First-order Raman Gain Coefficient	$g_{R1}(km^{-1}W^{-1})$	41.9
Second-order Raman Gain Coefficient	$g_{R2}(km^{-1}W^{-1})$	37.8

Figure 2 illustrate the forward- and backward propagation of the first and second Stokes waves. Reflectivity of the FBG_0 at 1064 nm is highly (around 99%) and pump power is 4 W. These figures show forward propagation of first and second Stokes waves around 2.2 W and 900 mW in low reflectivity fiber end mirrors and L=30 m, respectively.

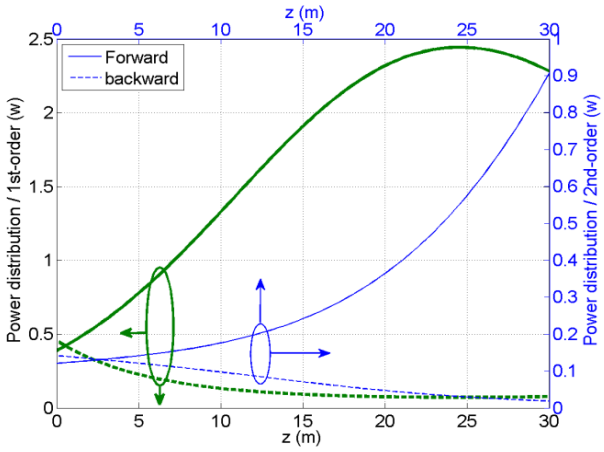

Figure 2. Forward- and backward distribution of the first Stokes wave and second Stokes wave in the HNL-PCF length for the grating-free Raman fiber laser.

Threshold pump powers of the 1st- and 2nd-order as a function of output reflection coefficient for various length of cavity and threshold pump power as a function of HNL-PCF length is shown in Figure 3.

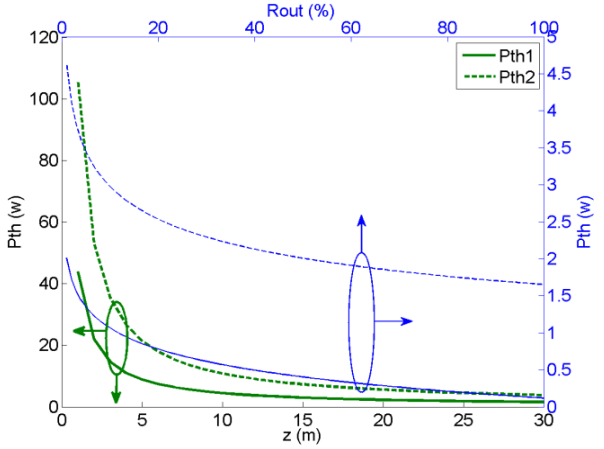

Figure 3. Threshold power for the first- and second-orders Stokes waves and as output reflection coefficients in the length of PCF for the grating-free RFL

According to the Table 2, these values for grating-free and Bragg grating HNL photonic crystal fiber are different. Threshold pump powers are less in the Bragg grating case and it can lased in more than the P_{th2}=0.7 W.

The transmitted pump power inside the PCF and forward-propagating for 2nd-orders of Stokes waves as input pump power grating-free Raman fiber laser made with HNL-PCF is indicated in Figure 4. Qualitative changes of laser characteristics occur at three sections. In first region incidence power below the P_{th1}=1.6 W. Maximum transmission power is around 1.5 W when input power is equal to the 1st-order threshold power. The second regime located between the P_{th1} and P_{th2}=3.8 W. The first Stokes radiation generates and increases with increasing pump power [9] and cavity starts lasing. Third region has been located above P_{th2}. The second order Stokes wave of the output power has been appeared in this region at first time. So changes of the output power curve for the second order Stokes wave has been shown in this region [9,12,13]. Extreme fluctuations of the optical power and unstable behavior during lunched pump power inter-cavity is explained by the rapid growth of the first-order Stokes wave so that decrease pump power at P_{th1}, consequently. Output power of the 1st-order Stokes wave is around 2.8 W when input power equal 2nd-order threshold power. As well as, the rapid growth of the second Stokes wave caused by decrease power of the first Stokes wave at P_{th2} [1].

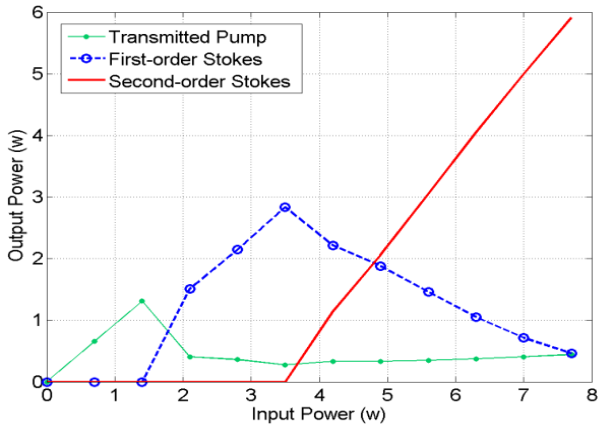

Figure 4. The transmitted pump power and forward propagation powers of the Stokes waves versus variable input power for the grating-free RFL based on HNL-PCF

In the partial FBGs, just some of the input power has been exchanged to the first-order output power. In this way, first-order output power has been exchanged to the second-order output power.

Table 2. Simulation Results of the Raman Fiber Laser Based on HNL-PCF

Parameters	**Values**	
	Grating free	Bragg grating
L (m)	30	60
R_{in1} (%)	85	30
R_{in2} (%)	85	30
R_{out1} (%)	3	65
R_{out2} (%)	3	30
P_{th1} (W)	1.6	0.4
P_{th2} (W)	3.8	0.7
P_{out1} (W)	2.21	0.28
P_{out2} (W)	0.88	0.59

Increase of attenuation process and measurements of the transmitted power in the HNL-PCF when P_{in} = 4, 6 and 8 W

as shown in Figure 5. Optical gain in the Raman cavity is decreased by increasing Pin, gradually.

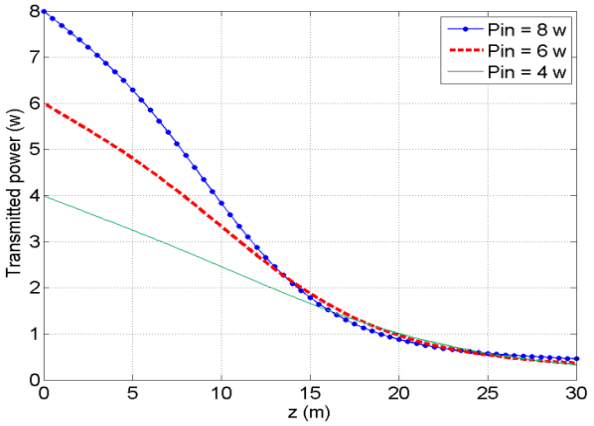

Figure 5. Transmitted pump power profile in the length of HNL-PCF for the grating-free RFL with several different input powers

Figure 6 illustrates shift in the first-order output power curve. The increase in output power caused by calculation differential equations with both orders of Stokes for the input pump power higher than 4 W. Therefore number of require stimulated carriers for positive gain become high. After this, loss increased for higher length in constant input pumping, regularly.

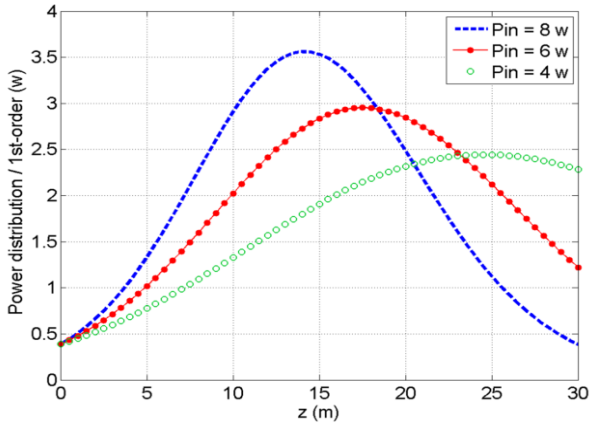

Figure 6. The first order Output power curves in the HNL-PCF length for grating-free RFL with different input pump power values.

As long as transferred of optical power in fiber, P_{out} gradually increased. With perfect population inversion, stimulated emission can dominate and increase of optical gains photon generated by stimulated emission in the cavity is attenuation and power energy oscillated. Population inversion is realized and the region exhibits optical gain [8,14]. When pump doesn't have enough energy to create a complete population inversion phenomenon in the low lunched pump power, gain starts to decrease in the length greater than 25 m. If the optical gain is not large enough to compensate for the cavity losses, the photon population cannot be built up [8]. Therefore, gain saturation and the first-order propagating wave eventually decrease, and insertion loss increases along the HNL-PCF length. Therefore, the effective length of HNL-PCF is set between 25 m to 30 m.

As observed from Figure 7, second-order output power is the least value when Pin=4 W. Also, most of the injection power is converted to the first-order output power in the length of active region for the grating-free RFL case.

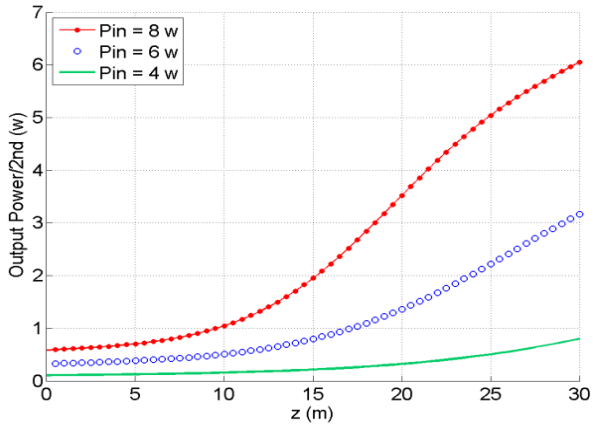

Figure 7. Output powers of the second-order forward propagation Stokes wave in the length of PCF with different input pump power values

Logical overlap between the curves based on R_{out1} and T_{out1} before fiber-end facet has been observed in Figure 8. In grating-free condition, total forward- and backward propagation of the first Stokes waves aren't more than 3.25 W. On the other hand, with increasing R_{out1} until 35% forward propagating wave is more than backward propagating wave. Forward propagation remains higher than backward propagation with growing R_{out1}. Therefore, difference between amounts of forward- and backward propagation radiation is increased.

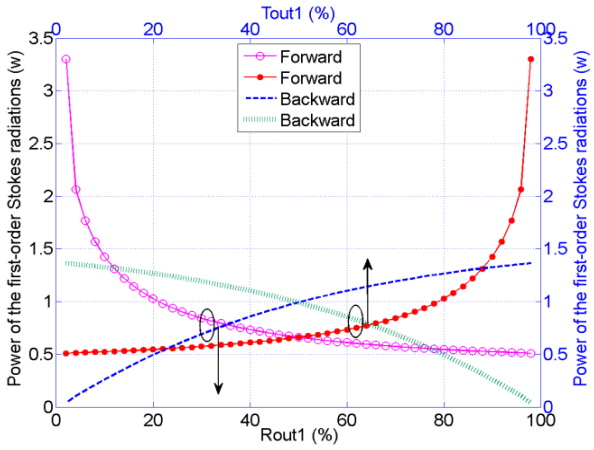

Figure 8. The power propagation of the first-order Stokes wave at λ_p=1064 nm, λ_{s1}=1118 nm, λ_{s2}=1177 nm versus transmission- and reflection coefficients for grating-free RFL before fiber-end facet

As described in Figure 3, minimum P_{th} can be found from the point of maximum R_{out} but this happen is limited by the results of Figure 9. Also, there is trade-off between output reflectivity and insertion loss in the choice of suitable threshold power of the PCF length.

Figure 9 shows variable output powers of two orders Stokes waves after fiber-end facet versus the first-order output transmission coefficient. In this case, maximum output power is around T_{out1}=97%.

Figure 9. Output power curves for different orders Stokes waves versus the first-order output transmission coefficient after fiber-end facet in the grating-free RFL

The maximum output power values as a function of the input pump power for first Stokes waves in grating-free and Bragg grating configurations are shown in Figure 10. Maximum output powers are around 2.45 W for grating-free and around 0.65 W for Bragg grating when P_{in}=4 W.

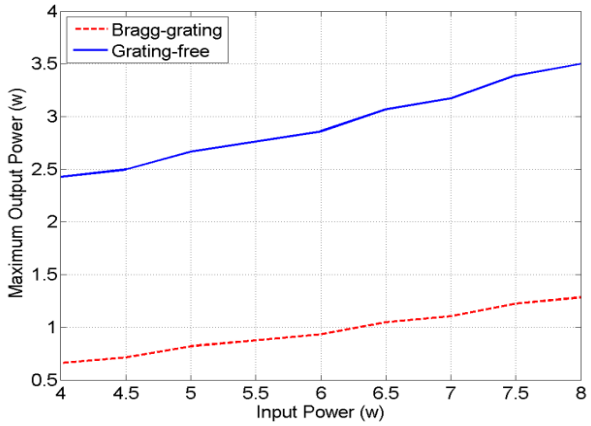

Figure 10. Maximum output power values as a function of the input pump power for with- and without Bragg grating represented by solid and dash lines, respectively

Therefore, the behavior of RFL with low-reflectivity FBG mirrors is changed similar to the amplification device. In this structure loss is less and output power is larger than the case with length of 25 m.

CONCLUSION

In this paper, we have simulated a new type of cascade Raman fiber laser made by HNL-PCF that can be used for the novel optical sources in optical communication. Using the numerical methods, we have analyzed the steady-state behavior of HNL-PCF based Raman fiber laser. The power threshold of the 2nd-orders Stokes waves, optical output powers curves and maximum output power functions versus input power with- and without reflectivity mirrors have been scrutinized. Furthermore, trade-off between optical output power and insertion loss in the length of laser is explained.

In this work, Laser has been optimized after tuning reflection coefficient before output facet for low-reflectivity. At last, we have proposed a new RFL with length of PCF about 30 m, R_{out1}=R_{out2}=30% and output power more than 2.2 W for input power 4 W. The results have been shown that the output power is high in the grating-free Raman fiber laser as compared to the Bragg-grating based RFL consists of a regular SMF with the same parameters. Also by comparing two types of HNL-PCFs based Raman fiber laser, we demonstrate that the length of grating-free Raman laser is shorter than another case.

REFERENCES

[1] S. Randoux, G. Beck, F. Anquez, G. Melin, L. Bigot, M. Douay, and P. Suret. 2009. Grating-Free and Bragg-Grating-Based Raman Lasers Made With Nonlinear Photonic Crystal Fibers. Journal of Lightwave Technology, vol. 27, no. 11, pp. 1580–1588.

[2] M.Rini, I.Cristiani, and V. Degiorgio. 2000. Numerical modeling and optimization of cascaded CW Raman fiber lasers. IEEE Journal of Quantum Electronics, vol. 36, no. 10, pp. 1117–2000.

[3] M. D. Mermelstein, C. Headly, J. C. Bouteiller, P. Steinvurzel, C. Horn, K. Feder, and B. J. Eggleton. 2001. Configurable Three-Wavelength Raman Fiber Laser for Raman Amplification and Dynamic Gain Flattening. IEEE Photonics Technology Letters, vol. 13, no. 12, pp. 1286–1288.

[4] Y. Wang and H. Po. 2003. Characteristics of fiber Bragg gratings and influences on high-power Raman fiber laser. Measurment Science and Technology, vol. 14, pp. 883–891.

[5] M. Fuochi, F. Poli, S. Selleri, A. Cucinotta, and L. Vincetti. 2003. Study of Raman Amplification Properties Triangular Photonic Crystal Fiber. Journal of Lightwave Technology, vol. 21, no. 1, pp. 2247–2254.

[6] M. Bottacini, F. Poli, A. Cucinotta, and S. Selleri. 2004. Modeling of Photonic Crystal Fiber Raman Amplifiers. Journal of Lightwave Technology, vol. 22, no.7, pp. 1707–1713.

[7] Headly C and Agrawal GP. 2005. Raman Amplification in fiber optical communication systems (Optics and Photonics), Elsevier Academic Press, London.

[8] Kelley PL, Kaminow IP, and Agrawal GP. 2001. Application of Nonlinear Fiber Optics, ser. Optics and Photonics, Academic Press: A Harcourt Science and Technology Company, London.

[9] C. Huang, Z. Cai, C. Ye, H. Xu, and Z. Luo. 2007. Optimization of dual-wavelength cascaded Raman fiber lasers using an analytic approach. Optics Communications, vol. 272, pp. 414–419.

[10] Y. Han. 2004. A long-Distance Remote Sensing Technique Using a Multiwavelength Raman Fiber Laser Based on Fiber Bragg Grating Embedded in a Quartz Tube. IEEE Sensors Journal, vol. 11, no. 5, pp. 1152–1156.

[11] M. Krause. 2007. Efficient Raman Amplifiers and Lasers in Optical Fibers and Silicon Waveguides: New Concepts, Ph.D. thesis, Technische Universität Hamburg-Harburg, Hamburg, Germany. Cuvillier Verlag, Göttingen, available online:urn:nbn:de:gbv:830-tubdok-5769.

[12] C. Huang, Z. Cai, C. Ye, H. Xu, and Z. Luo. 2007. Analytic modeling of the P-doped cascaded Raman fiber lasers. Optical Fiber Technology, vol.13, pp. 22–26.

[13] S. A. Babin, D. V. Churkin, and E. V. Podivilov. 2003. Intensity interactions in cascades of a two-stage Raman fiber laser. Optics Communications, vol. 226, pp. 329–335.

[14] Iga K and Kokubun Y. 2006. Encyclopedic Handbook of Integrated Optics, CRC Press, London.